PARP-1 inhibition with or without ionizing radiation confers reactive oxygen species-mediated cytotoxicity preferentially to cancer cells with mutant TP53

Qi Liu[1,6], **Liliana Gheorghiu**[1], **Michael Drumm**[1], **Rebecca Clayman**[1], **Alec Eidelman**[1], **Matthew F. Wszolek**[2], **Aria Olumi**[2], **Adam Feldman**[2], **Meng Wang**[1], **Lynnette Marcar**[1], **Deborah E. Citrin**[3], **Chin-Lee Wu**[4], **Cyril H. Benes**[5], **Jason A. Efstathiou**[1,*], and **Henning Willers**[1,*]

[1]Department of Radiation Oncology, Massachusetts General Hospital, Harvard Medical School, Boston, Massachusetts [2]Department of Urology, Massachusetts General Hospital, Harvard Medical School, Boston, Massachusetts [3]Radiation Oncology Branch, Center for Cancer Research, NIH, Bethesda, Maryland [4]Department of Pathology, Massachusetts General Hospital, Harvard Medical School, Boston, Massachusetts [5]Center for Cancer Research, Massachusetts General Hospital, Harvard Medical School, Charlestown, Massachusetts [6]Department of Radiation Oncology, University of California, San Francisco, California

Abstract

Biomarkers and mechanisms of poly (ADP-ribose) polymerase (PARP) inhibitor-mediated cytotoxicity in tumor cells lacking a BRCA-mutant or BRCA-like phenotype are poorly defined. We sought to explore the utility of PARP-1 inhibitor (PARPi) treatment with/without ionizing radiation in muscle-invasive bladder cancer (MIBC), which has poor therapeutic outcomes. We assessed the DNA damaging and cytotoxic effects of the PARPi olaparib in nine bladder cancer cell lines. Olaparib radiosensitized all cell lines with dose enhancement factors from 1.22 to 2.27. Radiosensitization was correlated with the induction of potentially lethal DNA double-strand breaks (DSB) but not with RAD51 foci formation. The ability of olaparib to radiosensitize MIBC cells was linked to the extent of cell kill achieved with drug alone. Unexpectedly, increased levels of reactive oxygen species (ROS) resulting from PARPi treatment were the cause of DSB throughout the cell cycle in-vitro and in-vivo. ROS originated from mitochondria and were required for the radiosensitizing effects of olaparib. Consistent with the role of *TP53* in ROS regulation, loss of p53 function enhanced radiosensitization by olaparib in non-isogenic and isogenic cell line models and was associated with increased PARP-1 expression in bladder cancer cell lines and tumors. Impairment of ATM in addition to p53 loss resulted in an even more pronounced radiosensitization. In conclusion, ROS suppression by PARP-1 in MIBC is a potential

Corresponding Author: Henning Willers, M.D., Dept. of Radiation Oncology, Massachusetts General Hospital, 55 Fruit Street, Boston, MA 02114. Tel. 617-726-5184, hwillers@partners.org.
*Co-Senior Authors

therapeutic target either for PARPi combined with radiation or drug alone treatment. The *TP53* and *ATM* genes, commonly mutated in MIBC and other cancers, are candidate biomarkers of PARPi-mediated radiosensitization.

Keywords

PARP-1; TP53; Radiosensitization; Muscle-invasive bladder cancer

Introduction

The poly (adenosine-diphosphate ribose) polymerase (PARP) family of nuclear and cytoplasmic proteins is involved in a multitude of cellular functions[21]. Of these proteins, PARP-1 is the most abundant isoform and a mainly nuclear protein that has emerged as an important target for anti-cancer treatments[16, 19, 42]. As a DNA-binding and chromatin-associating enzyme, PARP-1 mediates single-strand (ss) DNA break repair[48], alternative end-joining of DNA double-strand breaks (DSB)[2], and also aspects of homologous recombination (HR)[9]. Pharmacologic inhibition of PARP-1/2 is synthetically lethal with genetic or functional defects in BRCA1/2 and other genes in the HR pathway[7, 13, 18, 39]. A major underlying mechanism of cytotoxicity is the trapping of PARP-1, as well as PARP-2, molecules on ssDNA[39].

Inhibition of PARP-1 sensitizes malignant cells and tumors to ionizing radiation (IR), prompting its current testing in combination regimens with radiation therapy in clinical trials[20, 28, 30, 47, 51, 54]. The mechanisms through which PARP-1 inhibition causes radiosensitization are incompletely understood and predictive biomarkers of combination or drug alone treatments remain to be established[37]. Borgmann and colleagues reported that PARP-1 inhibition preferentially radiosensitized head and neck cancer squamous cell carcinoma (HNSCC) cell lines with functional defects in HR through interfering with DNA replication[54]. Similarly, Vens and colleagues found enhanced radiosensitization in BRCA2-defective cell lines while Mansour et al. implicated inhibition of alternative DSB end-joining in the radiosensitizing effect[28, 51]. Importantly, some of the anti-cancer effects of PARP-1 inhibitors may be mediated through mechanisms that are distinct from the commonly accepted model of synthetic lethality with defective HR[5, 17], raising the possibility that different PARP-1-dependent processes can modulate cellular resistance to IR.

Bladder cancer is the fifth most common cancer in the United States, and more than 90% are transitional cell carcinomas (TCC). About 75% of TCCs are superficial tumors while one quarter is muscle invasive bladder cancer (MIBC), which has a poor prognosis with high rates of distant metastases and long-term survival of only ~50%[26]. Novel treatment strategies for MIBC are thus needed. The Cancer Genome Atlas project has identified multiple genomic alterations in MIBC, including mutations in genes involved in DNA damage response and repair, *TP53*, *ATM*, and *ERCC2*[10]. In contrast to MIBC, superficial TCC have different genomic alterations including a lower percentage of *TP53* mutations[29]. Several potential targets for personalized biological or cytotoxic therapies are of interest in

MIBC and superficial TCCs50. However, to our knowledge, PARP-1 inhibition has not yet been explored as a therapeutic strategy in bladder cancer patients.

To characterize the radiosensitizing properties of targeted agents and discover associated genomic biomarkers we recently established a high-throughput cell line screening platform14, 33. For this approach, short-term radiosensitization using a 5-day cell survival/ proliferation endpoint was benchmarked against clonogenic survival in the gold standard colony formation assay. This design facilitates the screening of clinically relevant targeted agents at non-toxic concentrations and in conjunction with a clinical relevant dose of 2 Gy across dozens of cancer cell lines33. Here, we report our findings based on an initial screen of 9 TCC cell lines with the PARP-1/2 inhibitor olaparib. Unexpectedly, olaparib treatment with or without IR was preferentially cytotoxic to *TP53*-mutant but not wild-type cell lines derived from MIBC as well as other cancer types. Cytotoxicity was mediated by elevated mitochondrial ROS levels in MIBC in-vitro and in-vivo, suggesting a novel mechanism of PARP inhibitor activity that is distinct from ssDNA trapping.

Results

Sensitivity of bladder cancer cell lines to the PARP-1 inhibitor olaparib

As part of a larger cancer cell line screening effort using a high-throughput format for the testing of radiosensitizing targeted agents33, we observed varying degrees of radiosensitization by olaparib in nine mostly high-grade TCC cell lines, with radiosensitization factor (SRF_{2Gy}) values ranging from 1.02 to 1.35 (Fig. S1A, Fig. 1A). A similar spread of radiosensitization factors was found when validating findings in a clonogenic survival assay ($DEF_{SF0.1} = 1.25$-2.27) (Fig. 1A,B). Three cell lines, UM-UC-3, 5637, and 639-V, were particularly sensitive to olaparib with or without IR (Fig. 1A-C, S1B,C). The ability of olaparib to cause radiosensitization was closely correlated with cytotoxicity in drug alone-treated cells, suggesting a common underlying mechanism of effect (Fig. 1D, S1D).

Olaparib was particularly effective in causing γ-H2AX foci, thought to represent DSB, in UM-UC-3, 5637, and 639-V (Fig. 1E), and the number of these lesions correlated closely with cell kill (Fig. 1F). These data suggest that the ability of olaparib to cause DSB is closely related to the observed radiosensitization and drug alone effects. PARP inhibitors have been previously shown to cause synthetic lethality in cells with HR defects7. However, there was no apparent HR defect in the three most olaparib-sensitive cell lines as measured by RAD51 foci (Fig. 1G, Fig. S1E).

Increased reactive oxygen species (ROS) causally underlie the observed olaparib toxicity

When exploring potential mechanisms of olaparib sensitivity we observed an increase in ROS levels in olaparib-treated cells, which again was most pronounced in UM-UC-3, 5637, and 639-V cells (Fig. 2A). Interestingly, endogenous ROS levels and baseline γ-H2AX foci were already elevated in the olaparib-sensitive cell lines even in the absence of olaparib treatment (Fig. S2A,B). Upon exploring the kinetics of ROS and DNA damage formation during olaparib treatment, we observed that physical DNA strand breaks were already

detectable within 5 hours of drug treatment (Fig. 2B). Other measures of breaks, γ-H2AX and 53BP1 foci, showed kinetics indicating almost peak damage formation at 5 hours (Fig. 2C, upper panel). In contrast, ROS formation at 1 hour was nearly as pronounced as at 5 hours (Fig. 2C, lower panel), raising the possibility that ROS production was responsible for subsequent strand breakage and not merely a result of it. To determine whether increased ROS levels are a cause of DSB, we co-treated cells with a commonly used scavenger of ROS, N-acetyl cysteine (NAC). This resulted in a partial or full rescue of the olaparib-sensitive phenotype but had no effect in the relatively olaparib-resistant KU-19-19 cells (Fig. 2C, Fig. S2B). Furthermore, olaparib increased phosphorylation of Apoptosis Signal-Regulating Kinase 1 (ASK1) similar to hydrogen peroxide, and olaparib-induced apoptosis was blocked by NAC (Fig. S2C).

To confirm these findings in-vivo, we subjected a panel of 10 bladder cancer explants to olaparib treatment ex-vivo using a previously established protocol 4 (Fig. S3A,B). We observed inter-tumoral heterogeneity with regard to the ability of olaparib to induce γ-H2AX, with generally higher foci numbers seen in muscle-invasive as opposed to superficial tumors and normal cells (Fig. 3A,B, Fig. S3C). Mirroring our in-vitro findings olaparib treatment led to an increase in ROS which could be blocked by NAC and correlated with DSB induction (Fig. 3C-E). Consistent with the notion of a more pronounced pro-oxidant phenotype of MIBC, we observed that several genes involved in ROS metabolism, including *SOD2*24, were upregulated in invasive cancers compared to superficial tumors (Fig. 3F) or normal bladder (Fig. S3D). Together, the findings support a model in which MIBCs have an altered redox state that requires PARP-1 to regulate ROS levels.

Olaparib-mediated induction of DNA damage in the G1 phase of the cell cycle

In the synthetic lethality concept, PARP-1 molecules trapped at ssDNA breaks collide with DNA replication forks, thereby causing DSB that are detected in the S/G2 phases of the cell cycle. Accordingly, we treated cells with olaparib for only 5 hours to minimize cell cycle disruptions and apoptosis induction and then used flow cytometry to identify cells with high γ-H2AX expression (Fig. S4A). We detected an increased γ-H2AX signal throughout the cell cycle of olaparib-sensitive 639-V cells, including in cells in the G1 phase where no replication fork-associated DSB are expected (Fig. 4A). In contrast, barely any DSB induction was seen in olaparib-resistant KU-19-19 cells. To confirm this observation, we used serum starvation to block cell cycle progression. In the G1 phase-enriched 639-V cell population, olaparib readily caused DSB within 5 hours, in contrast to serum-starved KU-19-19 cells (Fig. 4B). In addition, using an immunofluorescence microscopy approach we co-stained 639-V cells for γ-H2AX and PCNA or 53BP1 and EdU to identify cells with DNA damage outside of S phase (Fig. S4B,C). Similarly, in olaparib-sensitive MIBC tissues, DSB containing cells frequently did not demonstrate S phase-typical PCNA staining, suggesting a G1 phase-specific event (Fig. 4C, Fig. S4D). Consistent with a replication-independent mechanism, a non-trapping PARP inhibitor was preferentially cytotoxic to 639-V cells (Fig. 4D). These data support a model in which elevated ROS levels in olaparib-treated cells cause cytotoxic DNA damage throughout the cell cycle including G1 phase.

Mitochondrial ROS are required for radiosensitization by olaparib

Next, to identify the source of the observed ROS increase in olaparib-treated cells, we employed a probe that specifically targets to mitochondria in live cells where it is oxidized by superoxide, the main mitochondrial ROS (Fig. 4E, left panel). We observed that olaparib caused a rapid increase in mitochondrial ROS (Fig. 4E, right panel), which mirrored the previously observed ROS kinetics (Fig. 2B). A mitochondria-targeted anti-oxidant reduced olaparib-induced ROS expression in cells and tumor tissue (Fig. 4D, F). In contrast, while an inhibitor of both mitochondrial and NAPDH oxidase (NOX) dependent ROS production was effective at ROS reduction, a NOX-specific inhibitor failed to suppress olaparib-induced ROS (Fig. S5A). As predicted, suppression of mitochondrial ROS reversed the olaparib sensitivity of TCC cells and tumors (Fig. 4G, Fig. S5B). Lastly, anti-oxidant treatment not only increased the resistance of cells to olaparib alone but also diminished olaparib-mediated radiosensitization, suggesting that increased mitochondrial ROS levels accounted for both effects (Fig. 4H, Fig. S5C).

Loss of wild-type p53 or ATM function sensitizes cancer cells to olaparib

When we surveyed the genomic profiles of our cell lines for potential biomarkers of olaparib effect we noticed that TCC lines that were strongly radiosensitized by olaparib were enriched for p53 core domain mutations (Fig. 5A,B). A similar trend was found when analyzing cancer cell lines of other histologies including non-small cell lung carcinoma (Fig. 5B,C). We confirmed this observation in several isogenic cell line models where loss of wild-type p53 resulted in increased sensitivity to olaparib with or without IR (Fig. 5D,E, Fig. S6A-C). As a transcription factor, p53 is known to be involved in redox regulation[35]. We, therefore, asked whether the previously observed reversal of olaparib sensitivity by an anti-oxidant is p53-dependent. NAC co-treatment increased cell survival of olaparib-treated p53-mutant but not isogenic wild-type cancer cells with or without IR (Fig. 5F, G). Consistent with this observation we also found a p53-mutant-specific increase in ROS upon olaparib treatment and a higher sensitivity of p53-mutant cells to oxidative stress compared to wild-type cells (Fig. 5H, Fig. S6D).

With regard to the mechanism of p53-dependent PARP inhibitor sensitivity, depletion of the p53-target gene product p21 did not sensitize p53 wild-type cells to olaparib, suggesting that the olaparib sensitivity of p53-mutant cells was not due to cell cycle perturbation (Fig. S6E). A recent report raised the possibility that the known HR suppressing function of p53 could affect PARP inhibitor sensitivity[25]. However, we found that a dissociation-of-function p53 mutant that has lost its transactivation function but maintained HR suppressive properties was unable to sensitize cancer cells to olaparib (Fig. S6F). Interestingly, we did observe increased expression of PARP-1 in p53-mutant TCC cell lines and tumors compared to wild-type (Fig. 5I, J), which is consistent with the idea that high ROS levels are associated with an increased dependence on PARP-1.

Lastly, we turned to the ATM kinase which acts upstream of p53, has a well-documented role in oxidative stress responses, and is mutated in a significant subset of MIBC and other cancers, sometimes even in conjunction with TP53 mutations[10]. We, therefore, evaluated the effects of disrupting ATM function on olaparib sensitivity in p53 wild-type versus deficient

cell line models. In cells where p53 function was impaired by the SV40 large T-antigen, the addition of ATM mutation led to a pronounced ROS increase upon treatment with olaparib, indicating that p53 and ATM independently affect PARP inhibitor sensitivity (Fig. 6A,B). ROS were also increased when ATM kinase was pharmacologically inhibited (Fig. 6C). Accordingly, the radiosensitizing effects of olaparib were more pronounced when both ATM and p53 functions were impaired compared to cells in which ATM status was unaltered (Fig. 6D,E, Fig. S7A). The olaparib sensitive phenotype of cells with mutant or pharmacologically inhibited ATM could be at least partially reversed by anti-oxidant treatment with NAC or MitoTEMPO (Fig. 6E, Fig. S7B,C).

Taken together, our data establish that elevated ROS in p53-mutant cells confer cellular sensitivity to olaparib with or without IR. Further loss of ATM kinase augments this sensitivity.

Discussion

There remains great interest in the utility of PARP inhibitors such as olaparib to sensitize human cancers to IR as well as other therapies[12, 37]. However, the extent of inter-tumoral variation with regard to the radiosensitzing effects of PARP inhibitors and biomarkers of radiosensitization are not well established. Biomarkers of drug alone effect in tumors not harboring BRCA mutations or a BRCA-like phenotype are also sparse[37]. Here, we report that olaparib radiosensitized the majority of cell lines derived from MIBC and other cancer types but with substantial heterogeneity across cell lines with regard to the magnitude of effect (Fig. 1A, 5C). Radiosensitization correlated with loss of p53 function in several isogenic and non-isogenic cell line models, indicating a cell line-independent phenomenon (Fig. 5A-D). Recent reports suggested that HR defects that normally associate with sensitivity to PARP inhibitor alone also confer sensitivity to combined IR/inhibitor treatment. For example, in a panel of 10 HNSCC cell lines, 5 lines with defective HR were preferentially radiosensitized by PARP inhibition (DEF of ~1.4-1.8), and at least 4 of them were p53-mutant[54]. Our data show that pronounced radiosensitization was achieved even in HR-proficient but p53-mutant TCC cells (DEF ~1.4-2.3) (Fig. 1G, 5A). Vice versa, a lung cancer cell line, NCI-H1563, which has a HR defect but is p53 wild-type, was not radiosensitized by olaparib (Fig. 1G, 5C)[33]. In another recent report studying radiosensitization in 9 cancer cell lines, the positive predictive effect of mutant/deleted p53 was less pronounced but entirely consistent with our data, i.e., mean DEF (range) for wild-type p53 = 1.25 (1.00-1.43) and for deficient p53 = 1.39 (1.25-1.61)[6].

Taken together, we propose that p53 status may be a useful biomarker, and potentially superior to HR status, for predicting the extent of radiosensitization by PARP inhibition. In contrast, p53 status had a relatively small influence on PARP inhibitor alone cytotoxicity compared to the drug sensitivity seen with HR-defective cells (Fig. 5E,F). Because in our data sensitivity to PARP inhibitor alone also predicted susceptibility to drug-induced radiosensitization, we suspected a common underlying mechanism of cytotoxic drug effect.

ROS are important for cell growth, stress adaption, and cell death in a concentration-dependent manner[22]. Because the cytotoxic effects of IR are partially mediated by free

radicals, high levels of cellular ROS are associated with enhanced radiosensitivity44. Furthermore, high ROS levels may also impair the ability of cells to cope with IR-induced damage. There exist multiple enzymatic and non-enzymatic sources of cellular ROS including mitochondria23, 40, 41. It is increasingly recognized that cancer cells often harbor high ROS levels to support proliferation and survival22. Yet, cancer cells may also be more sensitive to any further ROS increase and more prone to cell death because of it22, 36, 49. PARP-1 is a pleiotropic protein with numerous cellular functions. Interestingly, PARP-1 has been implicated in the regulation of mitochondrial function and oxidative metabolism3. Furthermore, it has been reported that PARP-1 resides in mitochondria where it is directly involved in mitochondrial DNA repair45. In a Parp-1 knockout mouse model, an increase in ROS levels was seen with age and a significant number of genes linked to oxidative stress and ROS production were misregulated compared to wild-type mice15. Thus, our data suggest that these lesser known roles of PARP-1 may yield potentially novel targets for anti-cancer treatment which to date have been underexplored.

The predictive value of p53 mutation for olaparib-mediated radiosensitization may therefore be explained by p53's role in regulating cellular ROS production35. For example, p53 has been reported to regulate ROS via its ability to modulate antioxidant gene expression including mitochondrial SOD2. Loss of p53 function may lead to cancer formation in part through increased ROS levels46. Accordingly, invasive bladder cancers accumulate TP53 mutations in contrast to superficial tumors29. In keeping with this observation, we observed functional and genomic evidence of an altered oxidant state in MIBC (Fig. 3) which correlates well with the previously described increased expression of SOD2 in invasive vs superficial and high-grade vs low-grade tumors24. SOD2 expression was also associated with metastatic potential in a pre-clinical bladder cancer model24.

Lastly, ATM deficient cells and tissues show increased levels of ROS and oxidative stress, and loss of ATM function is synthetically lethal with PARP inhibitor treatment8, 27. We found that ATM status was particularly important for olaparib-mediated radiosensitization in a setting where ROS were already increased due to p53 loss (Fig. 6). These findings have clinical relevance as *ATM* mutations occur in about 14% of MIBC, sometimes in conjunction with *TP53* mutations10. The data also suggest that combined ATM and PARP inhibitors constitute a useful treatment strategy in MIBC.

Taken together, our data support a model that provides mechanistic insight into the interplay between ROS production, PARP-1 function, and TP53/ATM status. This model explains how MIBC are characterized by a pro-oxidant phenotype due to TP53 loss (or/and impaired ATM function) and a hypothesized greater reliance on PARP-1 for controlling increased ROS production. PARP-1 inhibitor treatment for these cancers, with or without IR, may thus represent a promising biomarker-directed therapeutic strategy.

Materials and Methods

Cell lines and culture

Bladder cancer cell lines were obtained from the MGH/Sanger cancer cell line collection http://www.cancerrxgene.org/translation/CellLine or the ATCC. Cell cultures were passaged

for < 2 months after thawing an individual frozen vial. The identity of the cell lines had been tested as described using a set of 16 short tandem repeats (STR) (AmpFLSTR Identifier KIT, ABI). In addition, single nucleotide polymorphism (SNP) profiles based on a panel of 63 SNPs assayed using the Sequenom Genetic Analyzer was used for in-house identity checking whenever a cell line was propagated and confirmed uniqueness of cell lines for the ones without available STR33, 53. On some cell lines additional authentication was performed by Bio-Synthesis, Inc (Lewisville, TX). J82, TCC-SUP, 639-V, HT-1197, HT-1376 and UM-UC-3 were cultured in Dulbecco's modified Eagle's medium (DMEM), supplemented with nutrient mixture F-12 (all Sigma-Aldrich) and KU-19-19, 639-V, 5637, and T24 were maintained in RPMI-1640. A549 with/without p53 R273L, HCT116 with/without TP53 deletion, MCF-7 with/without HPV E6, AG01522, AT5BIVA, and NF cells were previously described 4, 32, 33, 52. All cell lines were tested for mycoplasma (MycoAlert, Lonza).

Human tumors

Tumor samples from patients with invasive or superficial bladder cancer were collected under a protocol approved by the Institutional Review Board. Fresh tissues were processed ex-vivo as described previously4. For genomic analyses, data from patients with bladder cancer were retrieved from The Cancer Genome Atlas through the cBioPortal for Cancer Genomics site11 or the Oncomine Cancer Microarray database 43.

Treatments

Olaparib (O9201) and KU-55933 (K5050) were purchased from LC Laboratories (Woburn, MA, USA), dissolved in Dimethyl Sulfoxide (DMSO, Sigma-Aldrich) to 10 mM or 20 mM, respectively, and stored at -80°C. 5 μM olaparib was used for in-vitro treatment unless otherwise indicated. Diphenyleneiodonium (DPI) and VAS-2870 were dissolved in DMSO, stored in -20°C, and used at 10 μM and 5 μM, respectively. Inhibitors were added to cells 1 hour before irradiation at desired concentrations. N-Acetyl-L-cysteine (NAC; Sigma-Aldrich, A9165) and MitoTEMPO (Sigma-Aldrich, SML0737) were dissolved in ddH2O and stored at -20°C. These compounds were aliquoted to avoid thaw-freeze cycles, with protection from light. ROS probes CM-H2DCFDA (DCF) and MitoSOX (Life Technologies) were dissolved in DMSO before each use to achieve concentrations of 10 mM and 5 mM, respectively. X-rays were produced by a Siemens Stabilipan 2 X-ray generator, which was operated at 250 kVp and 12 mA with a 2 mm Al filter, at a dose rate of 1.6 Gy/minute. Fresh human tumor samples were maintained in RPMI medium and treated within 2 hours of retrieval from patients with 10 μM olaparib or 10 Gy X-rays as a control, followed by incubation for 24 hours, embedding in OCT (Sigma Aldrich), and snap freezing in liquid nitrogen for later analysis.

Cell survival and proliferation assays

Clonogenic survival assays were performed as previously published33, 34. Determination of cell numbers at 5 days after irradiation was performed by using a fluorescent nucleic acid stain Syto60 or CellTiter-Glo (CTG) luminescence assay (Promega, Madison, WI) as described 33, 34.

Flow cytometry assays

Cell cycle distributions were investigated by standard flow cytometry analysis of DNA staining with propidium iodide (PI) (Sigma-Aldrich). In some experiments, cells were preincubated without serum for 48 hours, in orders to create a population enriched for cells in the G1 phase. Cells were collected and washed twice with PBS, and then fixed in 1% paraformaldehyde (PFA) and 80% ethanol. Cells were kept at -20°C until analysis. We co-stained cells with anti-γ-H2AX antibody (Millipore) to assess DNA damage across the cell cycle. Ethanol fixative was removed, and cells were permeabilized with 0.5% Triton X-100 in PBS. Following blocking in 5% goat serum, cells were incubated with γ-H2AX antibody for 2 hours. After twice washing in PBS, cells were incubated in Alexa-488 conjugated secondary antibody (Invitrogen). 1 mg/ml RNAse and 500 μg/ml PI was added at the end, and then analyzed by a LSRII flow cytometer (BD Biosciences).

Apoptotic cells were identified by AnnexinV as previously described 33. Cells were harvested 3 days after treatment. Suspended cells in the medium were also collected for analysis. Cells were spun down, washed twice with cold PBS, and resuspended in Annexin binding buffer with cell density adjusted to ~10^6/ml. Cells were stained with PI and Annexin V-FITC according to the manufacturer's protocol (BioVision).

Published protocols were used for flow cytometric detection of intracellular or mitochondrial ROS in living cells 1, 38. Briefly, cells were washed twice with Hank's Balanced Salt Solution (HBSS, Invitrogen), incubated with MitoSOX Red superoxide indicator diluted to 5 μM in HBSS for 30 minutes or 10 μM CM-H2DCFDA, followed by washing with HBSS. Costaining with 200 μg/mL PI was performed to exclude dead cells. Cells were scraped off the culture vessels and pushed through a mesh capped tube to promote single cell suspension. Cells were maintained on ice before flow cytometry analysis.

Immunofluorescence microscopy

Staining and visualization of DNA damage repair foci was essentially performed as described 52. Cells were plated on chamber slides to achieve subconfluency for fixing. Cells were fixed with 4% PFA, permeabilized with 0.5% TritonX-100, and blocked with 5% goat serum in PBS 0.1% TritonX-100 (all Sigma-Aldrich). Cells were incubated with anti-γ-H2AX mouse monoclonal antibody (Millipore; at 1:500 dilution), anti-53BP1 (Abcam; 1:500), anti-PCNA rabbit polyclonal antibody (Abcam; 1:200), or anti-RAD51 mouse monoclonal antibody followed by incubation with rabbit or mouse Alexa-488/-555 conjugated secondary antibody (Invitrogen) at 1:1,000. All slides were counterstained with DAPI, examined and photographed by fluorescence microscopy (Olympus BX51).

Cryosections from human tissue samples were fixed with 2% PFA for 15 minutes and permeabilized with 0.5% TritonX for 10 minutes afterwards. Following 1 hour blocking at room temperature with 5% goat serum/PBS, slides were incubated overnight with primary antibody in a humid chamber at 4°C. Mouse anti-PCNA was co-incubated with rabbit polyclonal anti-53BP1. Secondary antibody including goat anti-rabbit IgG (Alexa Fluor488, Invitrogen, 1:1000 dilution) and goat anti-mouse IgG (Alexa Fluor555, Invitrogen, 1:1000)

was incubated at room temperature for 1 hour. Slides were mounted in Fluoroshield with DAPI (Sigma, F6057).

Single-cell electrophoresis

Cells (1.5×10^5 cells/ml) were suspended in 1% low melting point agarose (CometAssay® LMAgarose, Trevigen, Cat#4250-050-02) in culture medium and transferred onto a frosted glass microscope slide. Slides were immersed in lysis solution (CometAssay® Lysis Solution, Trevigen, Cat# 4250-010-01) at 4°C overnight and then alkaline unwinding solution (NaOH 200 mM, EDTA 1mM, PH>13) at 4°C for 1 hour. Slides were placed in an electrophoresis tank containing alkaline electrophoresis buffer (NaOH 200 mM, EDTA 1mM, pH>13), subjected to electrophoresis for 30 min at 21~22 V (300 mA), washed with ddH2O, and fixed by 70% ethanol for 5 min, then stained with SYBR Gold. Tail moment was analyzed using TriTek CometScore™.

Western blotting

Western blotting was performed using standard methods. Specific primary antibodies were used against p53 (Santa Cruz; 1:200) and β-actin (Sigma; 1:1,000).

Statistics

Data presented in this manuscript were generally derived from three independent (biological repeats). Statistical comparisons were performed using GraphPad Prism 6.0 (GraphPad). The student's T-test was used assuming normal distributions. All tests were two-sided. No adjustments for multiple comparisons were made. Details on repeats and statistical tests are included in the Figure Legends.

Supplementary Material

Refer to Web version on PubMed Central for supplementary material.

Acknowledgement

References

1. Ameziane-El-Hassani R, Dupuy C. Detection of Intracellular Reactive Oxygen Species (CM-H2DCFDA). Bio-protocol. 2013; 3:e313.

2. Audebert M, Salles B, Calsou P. Involvement of poly(ADP-ribose) polymerase-1 and XRCC1/DNA ligase III in an alternative route for DNA double-strand breaks rejoining. J Biol Chem. 2004; 279:55117–55126. [PubMed: 15498778]

3. Bai P, Canto C, Oudart H, Brunyanszki A, Cen Y, Thomas C, et al. PARP-1 inhibition increases mitochondrial metabolism through SIRT1 activation. Cell Metab. 2011; 13:461–468. [PubMed: 21459330]

4. Birkelbach M, Ferraiolo N, Gheorghiu L, Pfäffle HN, Daly B, Ebright M, et al. Detection of Impaired Homologous Recombination Repair in NSCLC Cells and Tissues. J Thorac Oncol. 2013; 8:279–286. [PubMed: 23399959]

5. Brenner JC, Ateeq B, Li Y, Yocum AK, Cao Q, Asangani IA, et al. Mechanistic rationale for inhibition of poly(ADP-ribose) polymerase in ETS gene fusion-positive prostate cancer. Cancer Cell. 2011; 19:664–678. [PubMed: 21575865]

6. Bridges KA, Toniatti C, Buser CA, Liu H, Buchholz TA, Meyn RE. Niraparib (MK-4827), a novel poly(ADP-Ribose) polymerase inhibitor, radiosensitizes human lung and breast cancer cells. Oncotarget. 2014; 5:5076–5086. [PubMed: 24970803]

7. Bryant HE, Schultz N, Thomas HD, Parker KM, Flower D, Lopez E, et al. Specific killing of BRCA2-deficient tumours with inhibitors of poly(ADP-ribose) polymerase. Nature. 2005; 434:913–917. [PubMed: 15829966]

8. Bryant HE, Helleday T. Inhibition of poly (ADP-ribose) polymerase activates ATM which is required for subsequent homologous recombination repair. Nucleic Acids Res. 2006; 34:1685–1691. [PubMed: 16556909]

9. Bryant HE, Petermann E, Schultz N, Jemth AS, Loseva O, Issaeva N, et al. PARP is activated at stalled forks to mediate Mre11-dependent replication restart and recombination. EMBO J. 2009; 28:2601–2615. [PubMed: 19629035]

10. Cancer Genome Atlas Research N. Comprehensive molecular characterization of urothelial bladder carcinoma. Nature. 2014; 507:315–322. [PubMed: 24476821]

11. Cerami E, Gao J, Dogrusoz U, Gross BE, Sumer SO, Aksoy BA, et al. The cBio cancer genomics portal: an open platform for exploring multidimensional cancer genomics data. Cancer Discov. 2012; 2:401–404. [PubMed: 22588877]

12. Chalmers AJ, Lakshman M, Chan N, Bristow RG. Poly(ADP-ribose) polymerase inhibition as a model for synthetic lethality in developing radiation oncology targets. Semin Radiat Oncol. 2010; 20:274–281. [PubMed: 20832020]

13. Chan N, Pires IM, Bencokova Z, Coackley C, Luoto KR, Bhogal N, et al. Contextual synthetic lethality of cancer cell kill based on the tumor microenvironment. Cancer Res. 2010; 70:8045–8054. [PubMed: 20924112]

14. Coleman CN, Higgins GS, Brown JM, Baumann M, Kirsch DG, Willers H, et al. Improving the Predictive Value of Preclinical Studies in Support of Radiotherapy Clinical Trials. Clin Cancer Res. 2016; 22:3138–3147. [PubMed: 27154913]

15. Deschenes F, Massip L, Garand C, Lebel M. In vivo misregulation of genes involved in apoptosis, development and oxidative stress in mice lacking both functional Werner syndrome protein and poly(ADP-ribose) polymerase-1. Hum Mol Genet. 2005; 14:3293–3308. [PubMed: 16195394]

16. Dulaney C, Marcrom S, Stanley J, Yang ES. Poly(ADP-ribose) polymerase activity and inhibition in cancer. Semin Cell Dev Biol. 2017

17. Engert F, Schneider C, Weibeta LM, Probst M, Fulda S. PARP Inhibitors Sensitize Ewing Sarcoma Cells to Temozolomide-Induced Apoptosis via the Mitochondrial Pathway. Mol Cancer Ther. 2015; 14:2818–2830. [PubMed: 26438158]

18. Farmer H, McCabe N, Lord CJ, Tutt AN, Johnson DA, Richardson TB, et al. Targeting the DNA repair defect in BRCA mutant cells as a therapeutic strategy. Nature. 2005; 434:917–921. [PubMed: 15829967]

19. Feng FY, de Bono JS, Rubin MA, Knudsen KE. Chromatin to Clinic: The Molecular Rationale for PARP1 Inhibitor Function. Mol Cell. 2015; 58:925–934. [PubMed: 26091341]

20. Gani C, Coackley C, Kumareswaran R, Schutze C, Krause M, Zafarana G, et al. In vivo studies of the PARP inhibitor, AZD-2281, in combination with fractionated radiotherapy: An exploration of the therapeutic ratio. Radiother Oncol. 2015; 116:486–494. [PubMed: 26277432]

21. Gibson BA, Kraus WL. New insights into the molecular and cellular functions of poly(ADP-ribose) and PARPs. Nat Rev Mol Cell Biol. 2012; 13:411–424. [PubMed: 22713970]

22. Gorrini C, Harris IS, Mak TW. Modulation of oxidative stress as an anticancer strategy. Nat Rev Drug Discov. 2013; 12:931–947. [PubMed: 24287781]

23. Han D, Williams E, Cadenas E. Mitochondrial respiratory chain-dependent generation of superoxide anion and its release into the intermembrane space. Biochem J. 2001; 353:411–416. [PubMed: 11139407]

24. Hempel N, Ye H, Abessi B, Mian B, Melendez JA. Altered redox status accompanies progression to metastatic human bladder cancer. Free Radic Biol Med. 2009; 46:42–50. [PubMed: 18930813]

25. Ireno IC, Wiehe RS, Stahl AI, Hampp S, Aydin S, Troester MA, et al. Modulation of the poly (ADP-ribose) polymerase inhibitor response and DNA recombination in breast cancer cells by drugs affecting endogenous wild-type p53. Carcinogenesis. 2014; 35:2273–2282. [PubMed: 25085902]

26. Kamat AM, Hahn NM, Efstathiou JA, Lerner SP, Malmstrom PU, Choi W, et al. Bladder cancer. Lancet. 2016; 388:2796–2810. [PubMed: 27345655]

27. Kamsler A, Daily D, Hochman A, Stern N, Shiloh Y, Rotman G, et al. Increased oxidative stress in ataxia telangiectasia evidenced by alterations in redox state of brains from Atm-deficient mice. Cancer Res. 2001; 61:1849–1854. [PubMed: 11280737]

28. Kotter A, Cornils K, Borgmann K, Dahm-Daphi J, Petersen C, Dikomey E, et al. Inhibition of PARP1-dependent end-joining contributes to Olaparib-mediated radiosensitization in tumor cells. Mol Oncol. 2014; 8:1616–1625. [PubMed: 25028150]

29. Lamy A, Gobet F, Laurent M, Blanchard F, Varin C, Moulin C, et al. Molecular profiling of bladder tumors based on the detection of FGFR3 and TP53 mutations. J Urol. 2006; 176:2686–2689. [PubMed: 17085196]

30. Lee HJ, Yoon C, Schmidt B, Park DJ, Zhang AY, Erkizan HV, et al. Combining PARP-1 inhibition and radiation in Ewing sarcoma results in lethal DNA damage. Mol Cancer Ther. 2013; 12:2591–2600. [PubMed: 23966622]

31. Lee JS, Leem SH, Lee SY, Kim SC, Park ES, Kim SB, et al. Expression signature of E2F1 and its associated genes predict superficial to invasive progression of bladder tumors. J Clin Oncol. 2010; 28:2660–2667. [PubMed: 20421545]

32. Liu Q, Ghosh P, Magpayo N, Testa M, Tang S, Gheorghiu L, et al. Lung cancer cell line screen links fanconi anemia/BRCA pathway defects to increased relative biological effectiveness of proton radiation. Int J Radiat Oncol Biol Phys. 2015; 91:1081–1089. [PubMed: 25832698]

33. Liu Q, Wang M, Kern AM, Khaled S, Han J, Yeap BY, et al. Adapting a Drug Screening Platform to Discover Associations of Molecular Targeted Radiosensitizers with Genomic Biomarkers. Mol Cancer Res. 2015; 13:713–720. [PubMed: 25667133]

34. Liu Q, Wang M, Kern AM, Khaled S, Han J, Yeap BY, et al. Adapting a drug screening platform to discover associations of molecular targeted radiosensitizers with genomic biomarkers. Mol Cancer Res. 2015; 13:713–720. [PubMed: 25667133]

35. Maillet A, Pervaiz S. Redox regulation of p53, redox effectors regulated by p53: a subtle balance. Antioxid Redox Signal. 2012; 16:1285–1294. [PubMed: 22117613]

36. Martin-Cordero C, Leon-Gonzalez AJ, Calderon-Montano JM, Burgos-Moron E, Lopez-Lazaro M. Pro-oxidant natural products as anticancer agents. Curr Drug Targets. 2012; 13:1006–1028. [PubMed: 22594470]

37. Michels J, Vitale I, Saparbaev M, Castedo M, Kroemer G. Predictive biomarkers for cancer therapy with PARP inhibitors. Oncogene. 2014; 33:3894–3907. [PubMed: 24037533]

38. Mukhopadhyay P, Rajesh M, Yoshihiro K, Hasko G, Pacher P. Simple quantitative detection of mitochondrial superoxide production in live cells. Biochem Biophys Res Commun. 2007; 358:203–208. [PubMed: 17475217]

39. Murai J, Huang SY, Das BB, Renaud A, Zhang Y, Doroshow JH, et al. Trapping of PARP1 and PARP2 by Clinical PARP Inhibitors. Cancer Res. 2012; 72:5588–5599. [PubMed: 23118055]

40. Nisimoto Y, Diebold BA, Cosentino-Gomes D, Lambeth JD. Nox4: a hydrogen peroxide-generating oxygen sensor. Biochemistry. 2014; 53:5111–5120. [PubMed: 25062272]

41. Paxinou E, Weisse M, Chen Q, Souza JM, Hertkorn C, Selak M, et al. Dynamic regulation of metabolism and respiration by endogenously produced nitric oxide protects against oxidative stress. Proc Natl Acad Sci U S A. 2001; 98:11575–11580. [PubMed: 11562476]

42. Pommier Y, O'Connor MJ, de Bono J. Laying a trap to kill cancer cells: PARP inhibitors and their mechanisms of action. Sci Transl Med. 2016; 8:362ps317.

43. Rhodes DR, Yu J, Shanker K, Deshpande N, Varambally R, Ghosh D, et al. ONCOMINE: a cancer microarray database and integrated data-mining platform. Neoplasia. 2004; 6:1–6. [PubMed: 15068665]

44. Riley PA. Free radicals in biology: oxidative stress and the effects of ionizing radiation. Int J Radiat Biol. 1994; 65:27–33. [PubMed: 7905906]

45. Rossi MN, Carbone M, Mostocotto C, Mancone C, Tripodi M, Maione R, et al. Mitochondrial localization of PARP-1 requires interaction with mitofilin and is involved in the maintenance of mitochondrial DNA integrity. J Biol Chem. 2009; 284:31616–31624. [PubMed: 19762472]

46. Sablina AA, Budanov AV, Ilyinskaya GV, Agapova LS, Kravchenko JE, Chumakov PM. The antioxidant function of the p53 tumor suppressor. Nat Med. 2005; 11:1306–1313. [PubMed: 16286925]

47. Senra JM, Telfer BA, Cherry KE, McCrudden CM, Hirst DG, O'Connor MJ, et al. Inhibition of PARP-1 by olaparib (AZD2281) increases the radiosensitivity of a lung tumor xenograft. Mol Cancer Ther. 2011; 10:1949–1958. [PubMed: 21825006]

48. Strom CE, Johansson F, Uhlen M, Szigyarto CA, Erixon K, Helleday T. Poly (ADP-ribose) polymerase (PARP) is not involved in base excision repair but PARP inhibition traps a single-strand intermediate. Nucleic Acids Res. 2011; 39:3166–3175. [PubMed: 21183466]

49. Trachootham D, Alexandre J, Huang P. Targeting cancer cells by ROS-mediated mechanisms: a radical therapeutic approach? Nat Rev Drug Discov. 2009; 8:579–591. [PubMed: 19478820]

50. Van Allen EM, Mouw KW, Kim P, Iyer G, Wagle N, Al-Ahmadie H, et al. Somatic ERCC2 mutations correlate with cisplatin sensitivity in muscle-invasive urothelial carcinoma. Cancer Discov. 2014; 4:1140–1153. [PubMed: 25096233]

51. Verhagen CV, de Haan R, Hageman F, Oostendorp TP, Carli AL, O'Connor MJ, et al. Extent of radiosensitization by the PARP inhibitor olaparib depends on its dose, the radiation dose and the integrity of the homologous recombination pathway of tumor cells. Radiother Oncol. 2015; 116:358–365. [PubMed: 25981132]

52. Wang M, Morsbach F, Sander D, Gheorghiu L, Nanda A, Benes C, et al. EGF Receptor Inhibition Radiosensitizes NSCLC Cells by Inducing Senescence in Cells Sustaining DNA Double-Strand Breaks. Cancer Res. 2011; 71:6261–6269. [PubMed: 21852385]

53. Wang M, Kern AM, Hulskotter M, Greninger P, Singh A, Pan Y, et al. EGFR-mediated chromatin condensation protects KRAS-mutant cancer cells against ionizing radiation. Cancer Res. 2014; 74:2825–2834. [PubMed: 24648348]

54. Wurster S, Hennes F, Parplys AC, Seelbach JI, Mansour WY, Zielinski A, et al. PARP1 inhibition radiosensitizes HNSCC cells deficient in homologous recombination by disabling the DNA replication fork elongation response. Oncotarget. 2016; 7:9732–9741. [PubMed: 26799421]
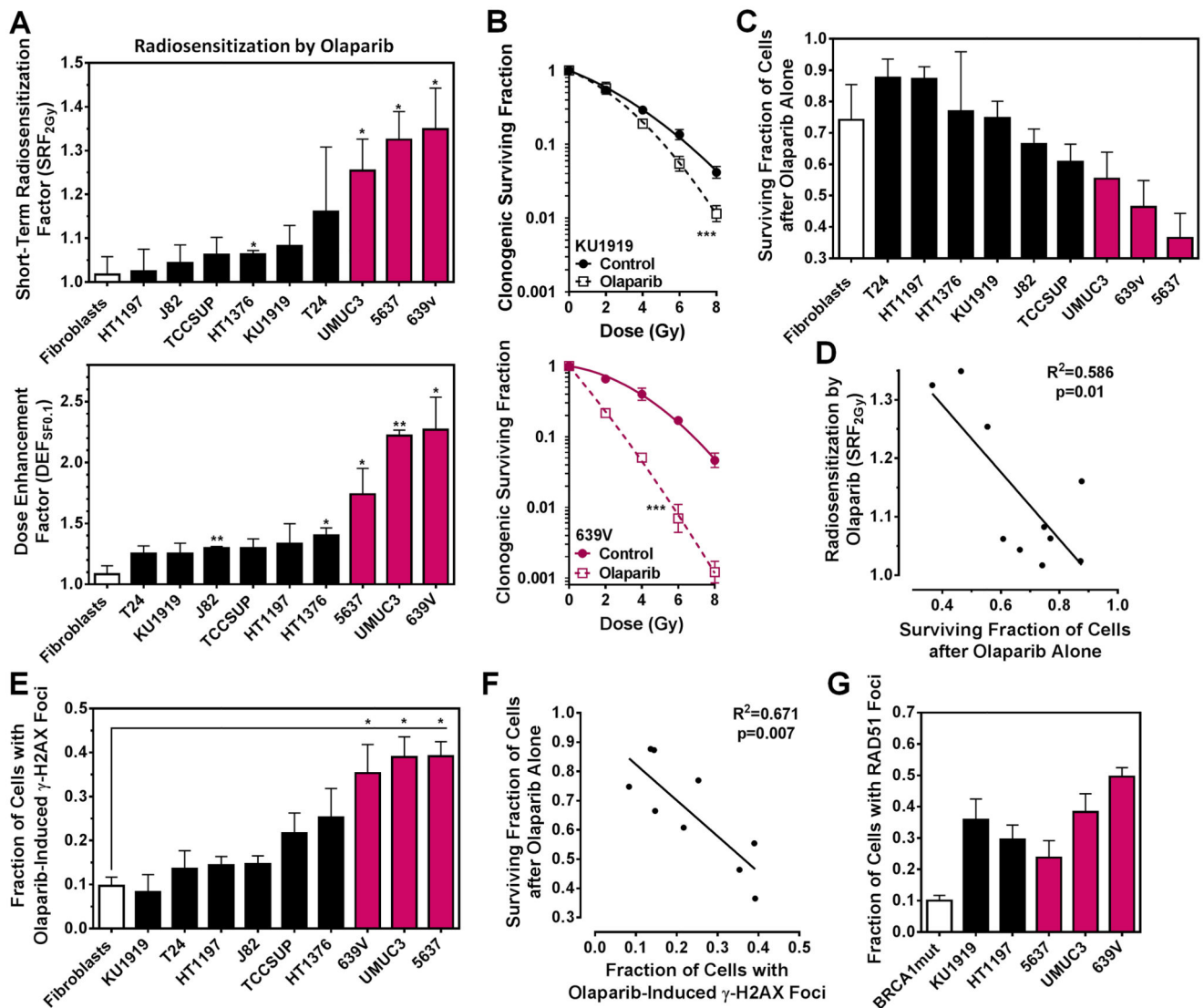
Figure 1. Sensitivity of transitional cell carcinoma (TCC) cell lines to the PARP inhibitor olaparib with or without ionizing radiation (IR) treatment.

A. Upper panel, short-term radiosensitization factors (SRF) for 9 TCC cell lines and fibroblast controls (AG01522) treated with 2 Gy and 5 μM olaparib in a plate-based screening format using the CTG assay 33. Lower panel, dose enhancement factors (DEF) at 0.1 survival fraction derived from full clonogenic survival curves fitted according to the linear-quadratic formalism. **B.** Illustration of clonogenic survival curves for an olaparib-resistant and -sensitive TCC cell line. **C.** Fraction of cells after treatment with 5 μM olaparib alone for 5 days using the syto60 assay 38. **D.** Correlation of SRF2Gy factors (A, upper) with drug alone toxicity (C). **E.** Fraction of cells with at least 20 γ-H2AX foci after 24 hours of olaparib treatment. **F.** Correlation of cell survival after olaparib alone (C) with γ-H2AX positivity (E). **G.** Fraction of cells with at least 10 RAD51 foci following olaparib alone treatment. BRCA1mut corresponds to HR-deficient control cell line (NCI-H1563). All bars or data points represent means based on at least 3 independent repeat experiments and error

bars indicate standard error. Statistical comparisons were made using the student's T-test (for pair wise comparisons and differences from 1), except for comparisons between survival curves (F-test) and linear regression analyses. *, p 0.05; **, p 0.01; ***, p 0.001.
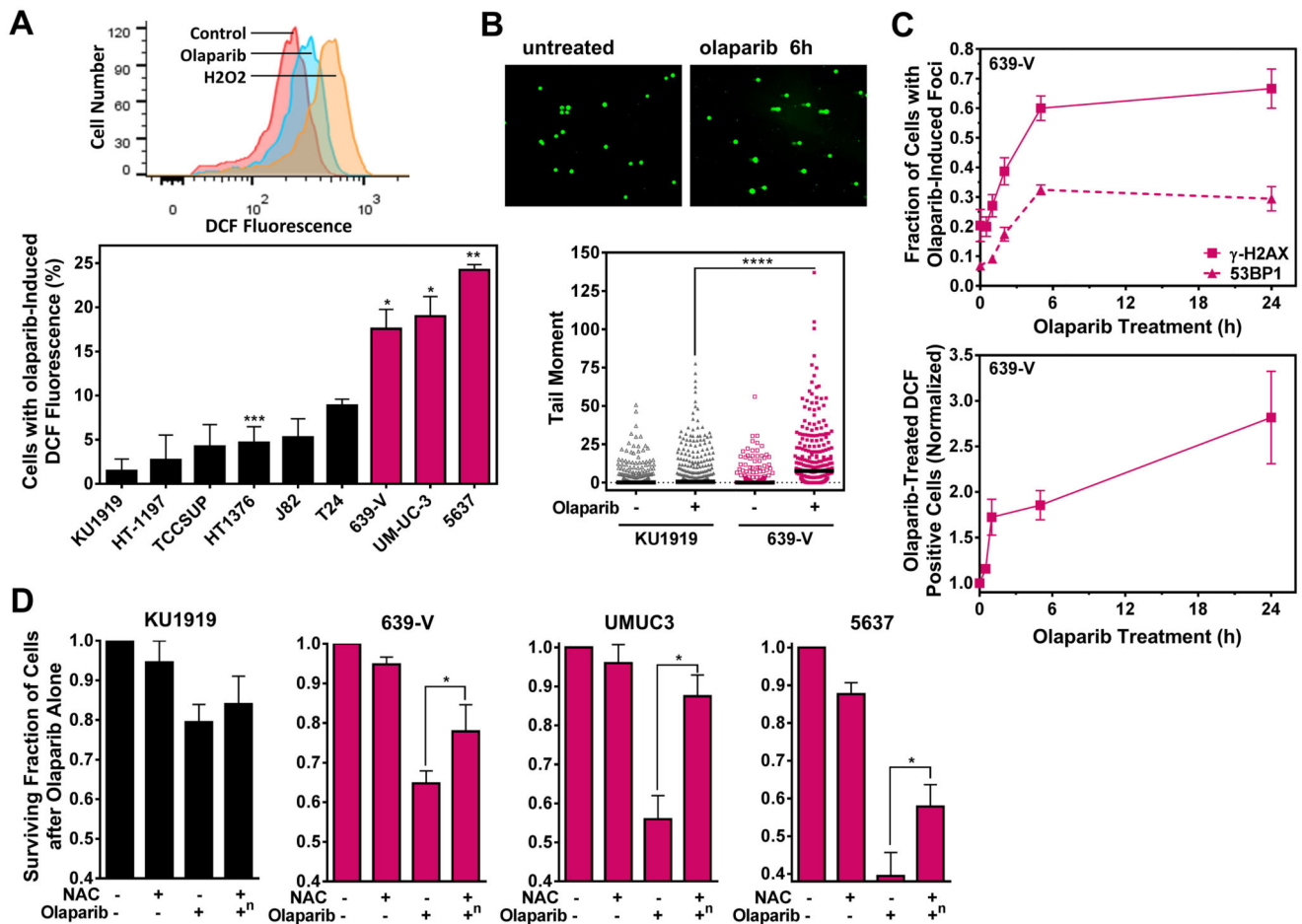
Figure 2. Involvement of ROS in olaparib-mediated cytotoxicity.
A. Upper panel, representative flow cytometry histograms to illustrate the olaparib-induced shift of ROS levels as detected by the DCF probe in 639-V cells. A 1 hour treatment with 100 μM H_2O_2 was used as a positive control. Lower panel, percentage of cells with high ROS levels following olaparib treatment, correct for endogenous ROS levels in the absence of drug. **B.** Upper panel, representative images illustrating olaparib-induced comets in 639-V cells following 5 hours (h) of drug treatment. Lower panel, quantification of alkaline Comet assay with tail moment plotted against treatments as indicated. Scatter plots show individual data points from 3 independent repeat experiments, with horizontal lines indicating median values. **C.** Upper panel, DSB kinetics using γ-H2AX and 53BP1 foci formation in olaparib-treated 639-V cells with readouts normalized to untreated controls. Lower panel, parallel determination of ROS formation. **D**. Fraction of cells after treatment with the anti-oxidant N-acetyl cysteine (NAC) or olaparib was determined by the syto60 assay. The combined drug effect was corrected for the effect of NAC alone as indicated by "n". NAC was added to cells every 24 hours at 0.5 mM (KU1919, 639-V) or 0.2 mM (5637, UMUC3). For data presentation and statistical comparisons see Fig. 1, except in Fig. 2B statistical comparison was performed using the Mann-Whitney test.
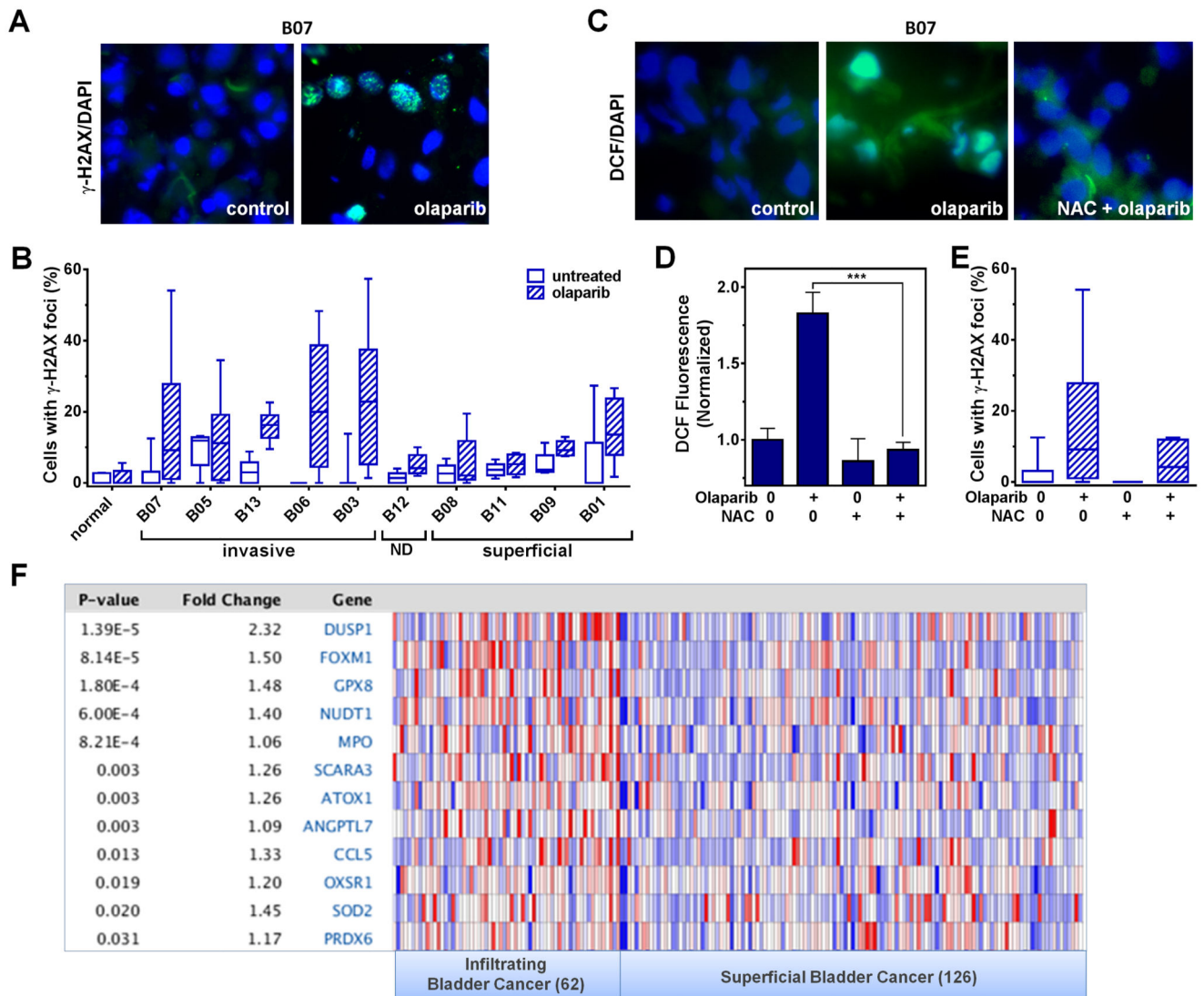
**Figure 3. Olaparib effects and ROS in human bladder tumors.**
A. Representative images demonstrating γ-H2AX foci induction in a MIBC explant. Blue, nuclear DAPI stain. **B.** Percentage of cells with at least two γ-H2AX foci following ex-vivo treatment of tissue explants with 10 μM olaparib for 24 hours. Tissues were grouped as normal (normal bladder wall), muscle-invasive carcinoma, superficial carcinoma, and other carcinoma (not defined, ND). Data are displayed in a box-and-whiskers plot, which shows the median value, quartiles, and the range of the data points. **C.** Illustration of **c**ell-based analysis of DCF fluorescence in a representative MIBC explant exposed to olaparib (10 μM) or/and NAC (1 mM) for 24 hours. **D.** Quantification of DCF fluorescence signal with treatments as indicated. **E.** Percentage of cells with at least two γ-H2AX foci in the same tumor as a function of ex-vivo drug treatment as indicated. **F**. Expression pattern of genes involved in the cellular response to oxidative stress in superficial (n=62) versus muscle-invasive bladder cancers (n=126) 31.
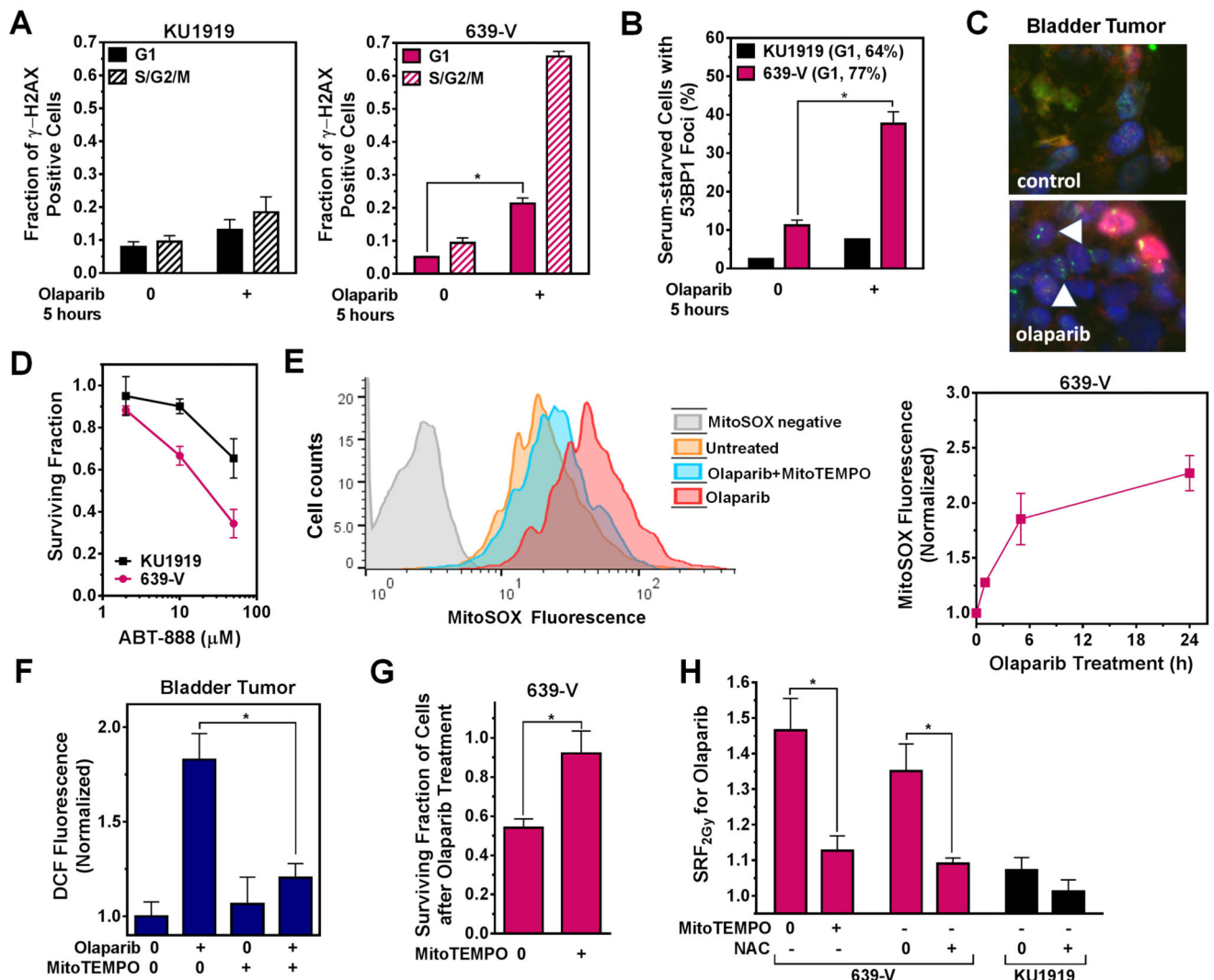
Figure 4. Effect of ROS on DNA damage and radiosensitization.
A. Fraction of cells with high γ-H2AX fluorescence after 5 hours (h) of treatment of olaparib. Fixed cells were co-stained with γ-H2AX and propidium iodide and analyzed by flow cytometry. Cells were divided into G1 phase or S/G2/M phase subgroups for quantifying γ-H2AX fluorescence. **B.** Percentage of cells with at least 20 53BP1 foci following 48 h of serum starvation +/- 5h olaparib, which led to an enrichment of the cell population with G1 phase cells. **C.** Representative images showing olaparib-induced 53BP1foci (green) in PCNA (red) negative cells in a MIBC explant. Arrows point to PCNA-negative cells harboring DSB, presumed to be in G0 or G1 phase. **D.** Sensitivity of 639-V and KU-19-19 cells to the catalytic non-trapping PARP inhibitor ABT-888 as measured by a 6-day cell proliferation assay (syto60). **E.** Left panel, Representative flow cytometry image showing MitoSOX fluorescence in 639-V cells under different conditions. Right panel, Kinetics of mitochondrial ROS as measured with the MitoSOX probe. **F.** Effect of a mitochondrial ROS scavenger (MitoTEMPO, 1 μM) on olaparib-induced ROS production in a MIBC explant analogous to Fig. 3D. **G.** Cell survival fraction of olaparib-treated 639-V

cells with or without MitoTEMPO as measured by the syto60 assay. **H.** Radiosensitization factors (SRF_{2Gy}) for representative olaparib-treated bladder cancer cell lines with or without MitoTEMPO or NAC co-incubation. For data presentation and statistical comparisons see Fig. 1.
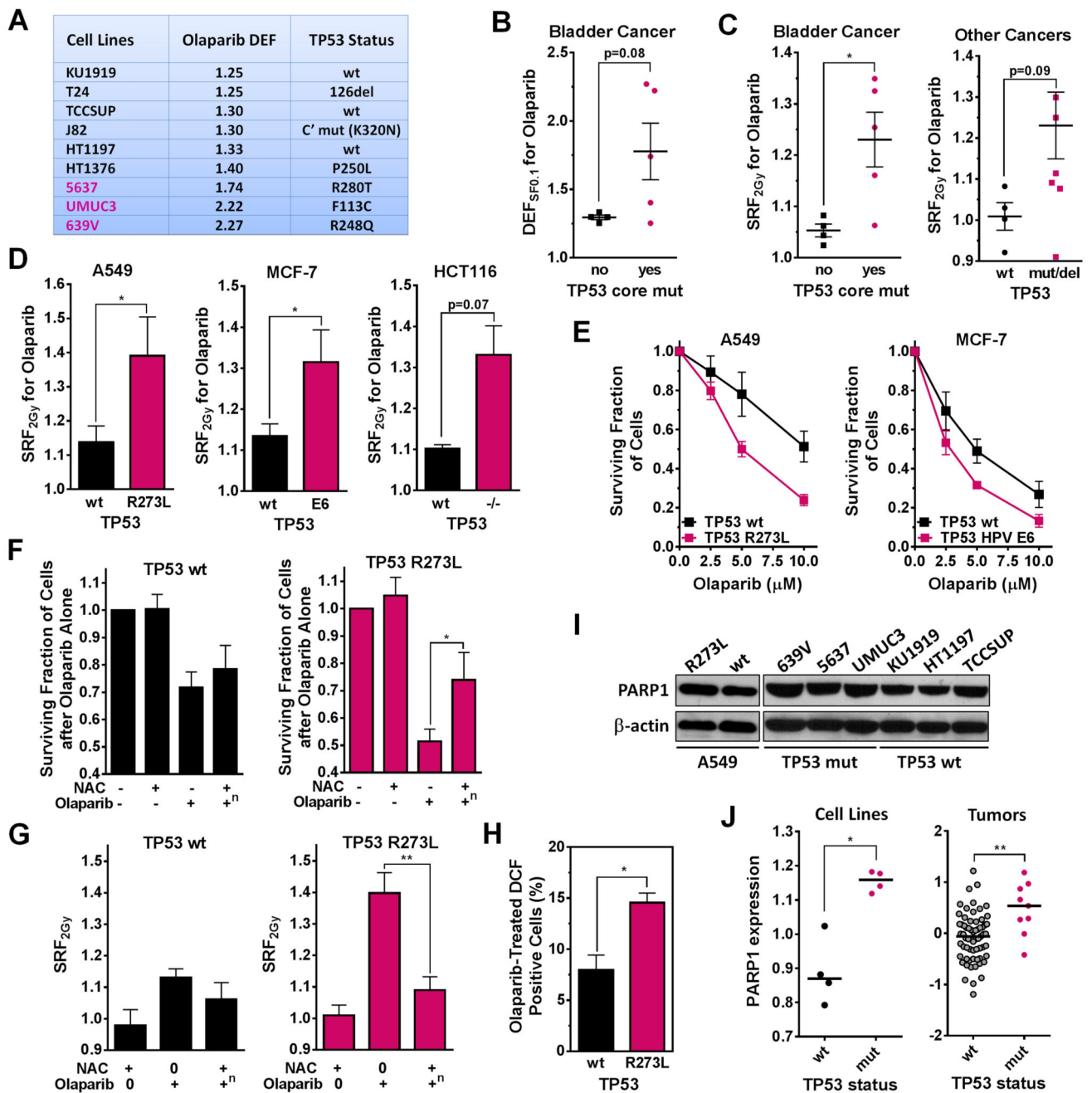
Figure 5. Role of TP53 status for olaparib-mediated ROS levels and cytoxicity.
A. Correlation of radiosensitzing effect by olaparib (DEF, dose enhancement factor) and curated TP53 mutation status (cancerrxgene.org/translation/CellLine, p53.free.fr). **B.** $DEF_{SF0.1}$ radiosensitization values for TCC cell lines with versus without mutations in the TP53 core domain. **C.** SRF_{2Gy} radiosensitization values for TCC cell lines (left panel) compared to cell lines from other cancer types (right panel). **D.** Comparison of SRF_{2Gy} values in isogenic cell pairs with variable TP53 status. wt, wild-type; R273L, mutant transgene; E6, HPV16 E6 infected; -/-, allelic knock-out. **E.** Fractions of A549 and MCF-7

cells treated with olaparib at the concentrations indicated for 5 days as measured by syto60 assay. **F.** Fraction of A549 cells following the treatments as indicated. The combined drug effect was corrected for the effect of NAC alone as indicated by "n". **G.** SRF_{2Gy} values for the treatments indicated are shown. **H.** Percentage of A549 cells with DCF fluorescence analogously to Fig. 2A. **I.** Whole cell lysates from the isogenic A549 pair and six TCC cell lines were subjected to Western blot for expression of PARP-1. **J.** Left panel, PARP1 protein bands from panel I were quantified with ImageJ and normalized to their corresponding β-actin expression values. Right panel, log-transformed PARP1 expression in a cohort of 74 patients with bladder cancer according to TP53 status [43]. For data presentation and statistical analysis, see Fig. 1, except for panel J for which the Mann-Whitney test was used.
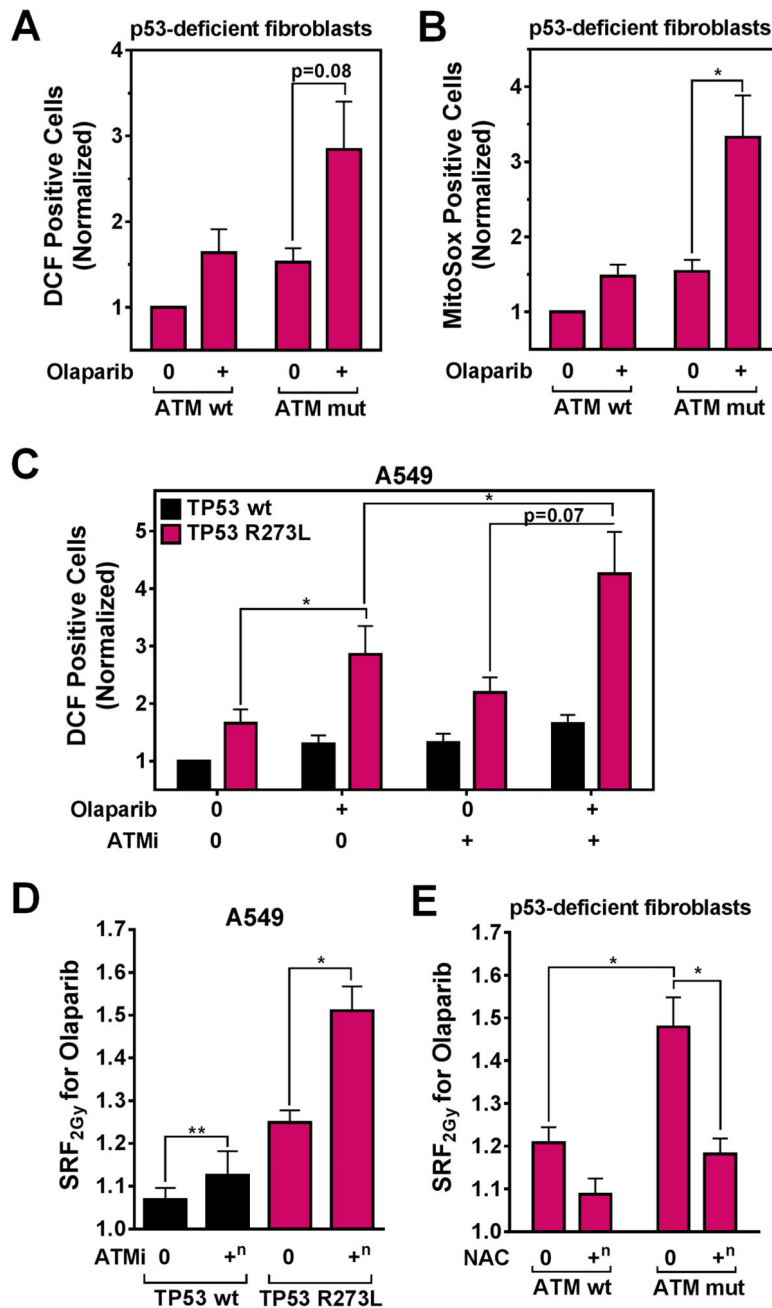
Figure 6. Role of ATM function for olaparib-mediated ROS levels and cytotoxicity.
A. Normalized DCF fluorescence of SV40-transformed human fibroblasts with non-functional p53 and either wild-type (wt, NF) or bi-allelic mutant (mut, AT5BIVA) for ATM, analogous to Fig. 2B **B.** Normalized MitoSOX fluorescence analogous to Fig. 4E. **C.** Normalized DCF fluorescence in isogenic A549 cell lines after treatments as indicated. ATMi, ATM inhibitor KU55933 used at 0.5 μM. **D.** SRF_{2Gy} radiosensitization values derived from the treatment of A549 tumor spheres 33. Combined drug effects were corrected for the cytotoxicity seen with KU55933 alone. **E.** SRF_{2Gy} values derived from the treatment

of SV40-transformed human fibroblasts with different ATM status. For data presentation and statistical analysis, see Fig. 1.